sustainability

MDPI

Article

An Experimental Study on the Determination of Shale K_{IC} by Semi-Disk Three-Point Bending

Hongjian Wang [1,2], Wenchang Zhang [1], Zijiang Zhao [3,*], Zhendong Cui [4,5,*], Jian Li [1] and Hao Zeng [1]

[1] Research Institute of Petroleum Engineering Technology, Zhongyuan Oilfield Branch of Sinopec, Puyang 457000, China
[2] College of Earth Sciences and Engineering, North China University of Water Resources and Electric Power, Zhengzhou 450045, China
[3] China Railway Bridge Engineering Bureau Group Co., Ltd., Tianjin 300300, China
[4] Key Laboratory of Shale Gas and Geoengineering, Institute of Geology and Geophysics, Chinese Academy of Sciences, Beijing 100029, China
[5] Institutions of Earth Science, Chinese Academy of Sciences, Beijing 100029, China
* Correspondence: leehanglan@126.com (Z.Z.); cuizhendong@iggcas.ac.cn (Z.C.)

Abstract: In order to accurately test the K_{IC} of the vertical stratification direction of shale, a semi-circular bending specimen with a linear chevron notch ligament (LCNSCB) was designed. The minimum dimensionless stress intensity factor (Y^{*}_{min}) of the LCNSCB specimen was calculated by the finite element method and the slice synthesis method, respectively. Two sets of prefabricated samples of the LCNSCB specimen under arrester and divider mode were used to conduct three-point bending loading experiments. The dispersion of the measured K_{IC} value of the specimens was analyzed by standard deviation and coefficient of variation, and the reason that the K_{IC} dispersion of specimens in divider mode was larger than in arrester mode was discussed. Compared with the experimental data of the existing literature, the data of this experiment shows that the LCNSCB specimen can avoid the disadvantage of lower measured K_{IC} values due to a larger fracture processing zone featured in the CSTSCB and CCNBD specimens, combined with the merits of a shorter fracture processing zone of the SR or CR specimens, and the render measured the K_{IC} value to be closer to the material's true fracture toughness value. The narrow ligament of the LCNSCB specimen has a favorable crack propagation guiding effect, can generate consistent K_{IC} values, and could be used to accurately test the fracture toughness of rock material in vertical bedding direction.

Keywords: shale; mode-I fracture toughness; three-point bending; LCNSCB; stress intensity factor (SIF); dimensionless stress intensity factor Y^*

check for updates

Citation: Wang, H.; Zhang, W.; Zhao, Z.; Cui, Z.; Li, J.; Zeng, H. An Experimental Study on the Determination of Shale K_{IC} by Semi-Disk Three-Point Bending. *Sustainability* **2023**, *15*, 1863. https://doi.org/10.3390/su15031863

Academic Editor: Kaihui Li

Received: 5 December 2022
Revised: 16 December 2022
Accepted: 14 January 2023
Published: 18 January 2023

1. Introduction

The stress intensity factor K is always a very important domination parameter, especially in today's linear elastic fracture mechanics. It can reflect the singular property of the stress field around the crack tip and have a close relation with the available energy's release rate. This factor, K, which has the dimensions of stress × (crack length)$^{0.5}$, can be obtained by analysis. The critical value of K is called the plane strain fracture toughness, denoted by K_{IC}. Thus, K_{IC} is generally regarded as a parameter of the mechanical capability of the material. In addition, it can be assumed that the crack growth causing catastrophic damage will occur when the K value reaches K_{IC}. Hence, a structure can be viewed as in a safe state when K is no more than K_{IC}, such as in a destructed state when K exceeds K_{IC}. As an important parameter in the field of fracture mechanics, fracture toughness, which describes the material resistance to the pre-existing cracks propagation, can be obtained by a test of experiment and calculation [1,2]. Rock fracture mechanics is an interdiscipline of mechanics with geoscience and geotechnical engineering [3,4]. Its application is very extensive. In addition to construction, dams, nuclear power plant foundation, tunnels, and other geotechnical engineering, it also involves coal mining, shale gas development, hot dry rock development, and other energy engineering problems [5–7]. Most of the previous studies on fracture toughness focused on homogeneous rocks, but less on heterogeneous rocks [8]. Especially for rocks with obvious anisotropy, such as transversely isotropic rocks with bedding distribution, the existing testing methods cannot accurately determine the K_{IC} value of rocks in the vertical bedding direction. Se-Wook Oh [9] investigated the relationship between the microcrack-induced fracture toughness anisotropy and the loading rate dependency by conducting static and dynamic fracture toughness tests on the straight notched disc bend (SNDB) specimen of Youngju granite. The anisotropic behavior of rock can be scaled by its elastic wave velocity and fracture toughness. According to the fracture geometry visualized by the X-ray CT results, the K_{IC} is supposed to be dictated by the microstructure of each material. Moreover, the K_{IC} value of the tested rock has the anisotropic characteristic due to the grain distribution [10]. M. H. B. Nasseri [11] proposed a new test method aiming at the assessment of the correlation between fracture toughness (K_{IC}) and fracture roughness of two granitic rocks (Barre and Stanstead granites), which both have significant anisotropic properties in fracture toughness. Layered rocks, especially shale, are not similar to isotropic media consisting of uniformly distributed particles, such as sandstone. Because the mineral particles are arranged in the direction of the parallel plane, and the micro-cracks and pores formed during the generation and storage of gas are ubiquitous in its interior, its mechanical properties are characterized as anisotropy [12–16]. Due to the influence of rock sample structure and experimental test methods, the test results of rock fracture toughness are very discrete. Therefore, the International Society for Rock Mechanics recommended a variety of standard methods for testing rock fracture toughness [17–20]. Wang et.al prepared the CCNBD and CSTSCB specimens to test the fracture toughness of shale specimens at 0°, 45°, and 90° bedding angles [21]. This study also suggested that the tested results of K_{IC} were smaller and showed greater scatteredness for SCB shale specimens than those for CCNBD specimens, which can be interpreted by the differences in notch type and the fracture process zone. The test results of rock fracture toughness are affected by many factors, and many scholars have studied the test methods. However, the test methods and specimen configurations are relatively complex. Therefore, some scholars suggest that the rock fracture toughness should be tested by a straight-slit semi-circular disc specimen. This method not only saves rock samples but also reduces the difficulty of sample preparation [22–24]. Similar to the experimental results in the literature [25], the CSTSCB specimen did not have the phenomenon of fracture stripping along the horizontal layer. The reason may be that the experimental conditions of three-point bending loading can provide a sufficiently large stress concentration strength for the crack tip to ensure that the vertical propagation of the crack does not deviate from the symmetry plane. In reference [26], the prefabricated crack of the herringbone CCNSCB specimen has a certain guiding effect, which can reduce the probability of deflection of the prefabricated joint during the expansion process, but it cannot be completely avoided. The fracture load Pmax and the calculated fracture toughness K_{IC} values are somewhat improved in dispersion, but only to some extent close to the K_{IC} values representing the true properties of the shale; it is still necessary to continue to improve.

In this paper, a linear chevron-notched semi-circular bending specimen (abbreviated as LCNSCB) is designed to measure the fracture toughness of the layered rock in the vertical bedding direction. The Y^*_{min} of the test specimen with this grooved configuration was calculated by the finite element method and the slice synthesis method, respectively. The fracture toughness was tested by a three-point bending experiment to verify the validity of this configuration specimen.

2. Specimen Preparation and Testing

The configuration and loading configuration of the semi-disc three-point bending test specimen are shown in Figure 1. Formula (1) for calculating the fracture toughness is the same as the formula for calculating the fracture toughness of the CNNBD test specimen, regardless of whether the groove is an oblique straight groove (LCNSCB) or a herringbone groove (CCNSCB) cut by a saw blade. Unification is the formula suggested by ISRM [25].

$$K_{\mathrm{IC}} = \frac{P_{\max}}{B\sqrt{R}} Y^{*}_{\min} \tag{1}$$

(**a**) (**b**)

Figure 1. Sampling position. (**a**) Sampling location of shale rock and (**b**) outcrop shale with a layered joint.

In the formula, K_{IC} indicates the fracture toughness value of mode-I; $P_{\max}$ indicates the peak load; B is the thickness of the specimen; R is the radius of the specimen; $Y^{*}_{\min}$ is the minimum dimensionless stress intensity factor; and 2S is the support span.

The rock specimens used in this experiment are shale in Shizhu County, Chongqing. The outcrop shale is located at the exit of the Dafengao No. 3 tunnel in Shizhu County, Chongqing, as shown in Figure 1a; outcrop shale has layered joints. From the broken shale fragments on site, it can be preliminarily judged that the shale has high brittleness and low hardness, as shown in Figure 1b. For mechanical parameters, see the literature [21]. Loading and geometry configuration of LCNSCB is shown in Figure 2. The radius, thickness, and grooving size of the semi-disc specimen are listed in Table 1. The corresponding dimensionless dimension are $\alpha_0(=a_0/R)$, $\alpha_1(=a_1/R)$, $\alpha(=a/R)$, $\alpha_B(=a_B/R)$, and $\alpha_S(=S/R)$. Four specimens were prepared for cutting groove and bedding arrester arrangement, and four specimens for divider arrangement, respectively. The grooving configuration is shown in Figure 3a,b.

The schematic diagram of the V-shaped groove is illustrated in Figure 4. The V-shaped groove is processed by a diamond wire cutting machine, which can realize a prefabricated artificial seam with a width of 0.5 mm. When calculating the K_{IC} value, the stress distribution at the tip of the fine groove is closer to that of the sharp crack. Compared with blade cutting, wire cutting has many advantages in rock sample preparation. For example, the wire cutting slit width is small, reducing the damage degree of rock samples. In addition, wire cutting can ensure the flatness of the sample cutting surface and improve the test accuracy of rock fracture toughness. Finally, the sample preparation method is more convenient. The inclination angle of the specimen is set to θ, and the cutting line level is guaranteed. The cutting depth of the sample is Hc. During the line cutting operation, the cutting part needs to be water-cooled to prevent friction and thermal erosion from changing the fracture toughness of the rock cutting joint.

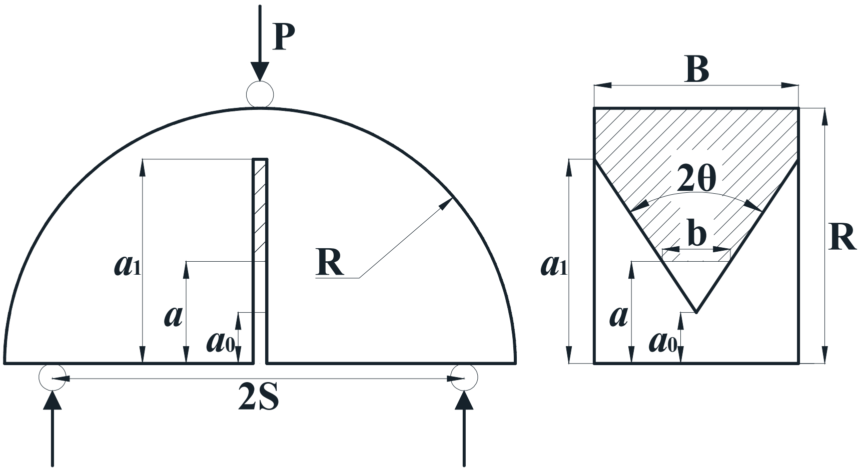

Figure 2. Loading and geometry configuration of LCNSCB.

Table 1. Geometry of the LCNSCB specimen.

Specimen Size Description	Value	Normalized Value
Radius R (mm)	37.5	–
Thickness B (mm)	30	0.8
Initial crack length a_0 (mm)	0	0
Termination crack length a_1 (mm)	37.5	1
Grooving angle 2θ (°)	43.6°	–
Support span $2S$ (mm)	60	0.8

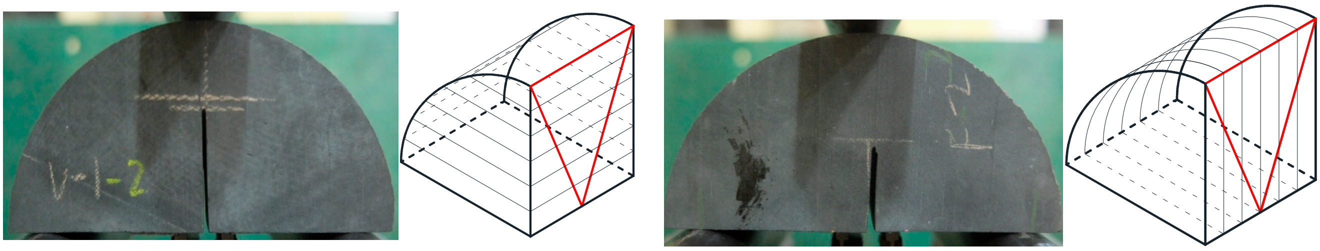

(**a**) arrester (**b**) divider

Figure 3. Ligament geometry of the LCNSCB specimen.

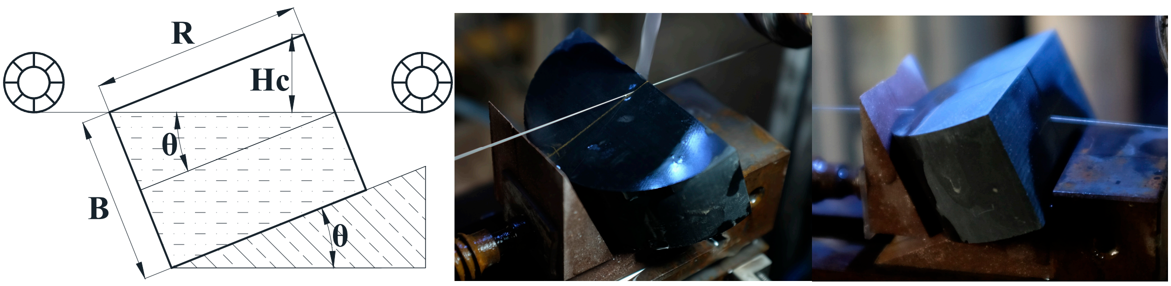

Figure 4. Machining of the LCNSCB notch.

The configuration of three-point bending loading is presented in Figure 5. The research group specially designed the loading system and supporting device for the three-point bending test. Loaded by the MTS-CMT5105 rock testing machine, the maximum load is 100 kN, and the loading rate is 0.06 mm/min. The specimens need to be accurately placed between the two rollers using alignment aids. Before the fracture mechanics test, auxiliary lines need to be drawn on both sides of the semi-circular specimen. The auxiliary lines include two horizontal lines and three vertical lines. The horizontal auxiliary lines are used to determine the position of the artificial cutting seam, and the vertical auxiliary lines are used to determine the position of the support point of the semi-circular specimen. These preparations ensure the accuracy of the experimental results.

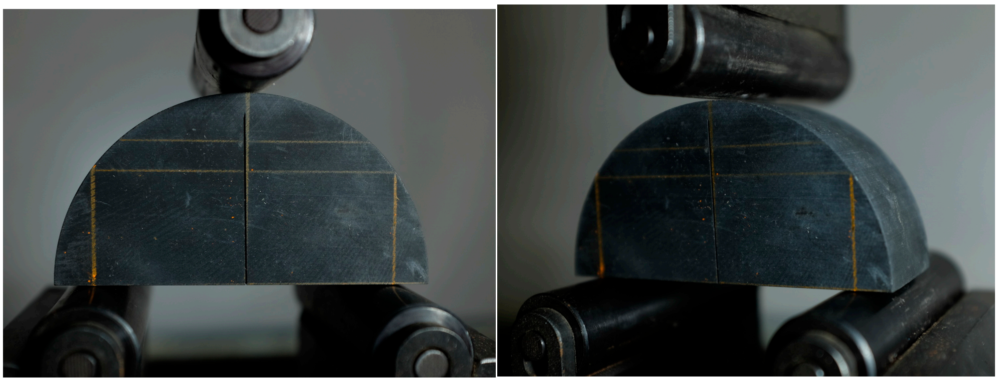

Figure 5. Configuration of three-point bending loading.

During the experiment, it is necessary to ensure that the manual slits are straight, the slits on the front and back of the sample are symmetrical, and the supporting points are symmetrical. In this way, the symmetry of the strain field and stress field at the crack tip can be ensured during the loading process. The purpose is to ensure the vertical propagation of the crack as much as possible and to avoid the inclined crack to the maximum extent.

3. Two Methods to Calculate Y^{*}_{min}

3.1. *The Finite Element Method*

A 3D model of semi disc specimen with a V-shaped groove was built using the ABAQUS method, and the dimensionless stress intensity factor (SIF) at the crack tip of the specimen was calculated. The J-integral can obtain the stress intensity factors of multiple confining channels around the crack. This method is used by many scholars to calculate the SIF of the herringbone groove specimen, which is considered to be effective and feasible [26,27].

Figure 6a is a specimen model established with ABAQUS. Using symmetry, only a half-mesh model is built to simulate the specimen. The model consists of approximately 50,000 units and 110,000 nodes. The elastic modulus and the Poisson ratio are set as 3.5 GPa and 0.3, respectively. The geometric configuration dimensions are listed in Table 1.

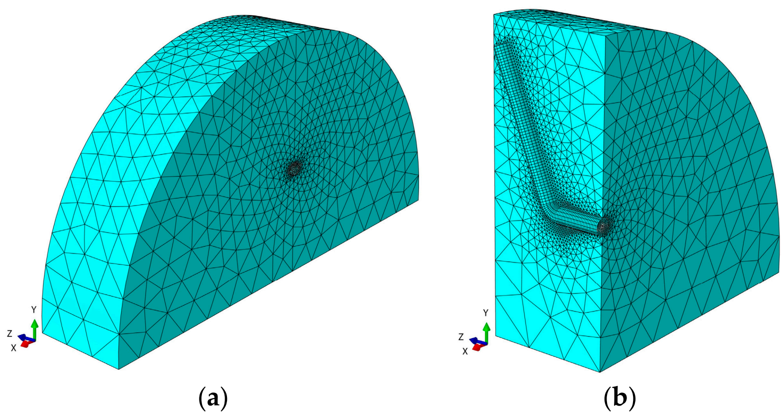

Figure 6. Meshing of the total model and crack ligament. (**a**) Model grid; (**b**) Fracture ligament mesh.

The area near the crack tip is finely divided by a hexahedral grid, and the remaining model is filled by a tetrahedral grid. Note that there exists mesh refinement near the crack tip to obtain the correct stress and strain, which solve the stress singularity problem near the crack.

The sharp corner at the junction of the straight crack in the middle of the V-groove crack front and the oblique crack on both sides is passivated to a rounded corner. This treatment can solve the problem of stress concentration at the sharp corner. The fillet radius is determined through multiple attempts, and finally, the K_{IC} values of the measuring points on the middle straight crack can be made more consistent.

A series of Y^* values with the corresponding varying crack length (a) can be obtained by setting the appropriate boundary limit for the numerical model and applying the appropriate load at the top of the specimen. The V-groove of the specimen is actually a three-dimensional configuration. The K_{IC} values of the nodes in the middle part of the crack front are not completely the same, and there are some differences. The average K_{IC} of the middle straight measurement point is taken as the corresponding K_{IC} when the crack length is a. This is a general numerical model calculation method for calculating the V-groove specimen K_{IC} at a given crack length (a). The finite element analysis can directly obtain the stress intensity factor K_{IC}. Then, the dimensionless stress intensity factor Y^* can be obtained by applying the calculated K_{IC}, load P, and geometric dimensions into Formula (1). Repeat this step to calculate Y^* corresponding to all selected α values. According to the series of points calculated above, the trend curve of Y^* with α is fitted to find the turning point of the curve. The critical crack length α_m and the corresponding minimum dimensionless intensity factor $Y^*{}_{min}$ can be obtained. In this example, Figure 6b shows the model when the crack length is α = 0.45. Figure 9 shows the Y^* curve obtained by the finite element method (FEM) fitting.

3.2. The Slice Synthesis Method

The slice synthetic method (SSM) was first proposed by Bluhm to calculate the stress intensity factor (SIF) of a V-grooved cube prism three-point bending specimen [28]. Xu and Fowell calculated the SIF of the CNCNBD specimen by the slice synthetic method [29]. Both of these are slice synthetic methods based on flexibility calculations. Wang QZ proposed a new method of slicing synthesis to calculate the SIF of a CCNBD specimen, which is simpler and more effective than the flexibility method by using the stress intensity factor directly instead of the flexibility [30].

Referring to Wang's slice synthesis method, the load of the LCNSCB specimen is equal to the load of a single CSTSCB specimen with an intermediate thickness b and the superimposed load of the N-piece thin CSTSCB specimen with a thickness Δt on both sides, as shown in Figure 7. Equation (2) gives the formula for calculating the fracture toughness of CSTSCB specimens, where Y' is the dimensionless stress intensity factor of CSTSCB specimens [31].

$$K_{IC} = \frac{P_{\max}\sqrt{\pi a}}{2RB}Y' \tag{2}$$

$$\begin{aligned} Y' &= 0.41 + 5.06(s/2R) + (-16.65 + 3.32(s/2R))(a/R) + \\ &(52.94 + 76.91(s/2R))(a/R)^2 + \left(-67.03 - 257.73\left(s/2R\right)\right)(a/R)^3 \\ &+(29.25 + 252.8(s/2R))(a/R)^4 \end{aligned} \tag{3}$$

During the crack propagation of the LCNSCB specimen, according to the assumption of a straight through crack, the crack front always maintains a straight shape and only the stress intensity factor in the middle straight crack zone remains basically unchanged; that is, the central part of the width (b) is a real crack [30]. The stress concentration of the notches on both sides is attenuated, so the stress intensity factor is smaller than the central straight crack. K'_I and K_I are taken to represent the stress intensity factors of the grooves on both sides and the grooves with straight cracks in the center width of b, respectively; then,

$K'_{\mathrm{I}} = K_{\mathrm{I}}/\beta$. Here, β is an empirical coefficient greater than 1. Assuming that the slot on the single side is divided into N slices, the load from the medial to the lateral number i slice is:

$$P_i = \frac{2R\Delta t K_{\mathrm{I}}}{\beta Y'(\alpha_i)\sqrt{\pi a_i}} \tag{4}$$

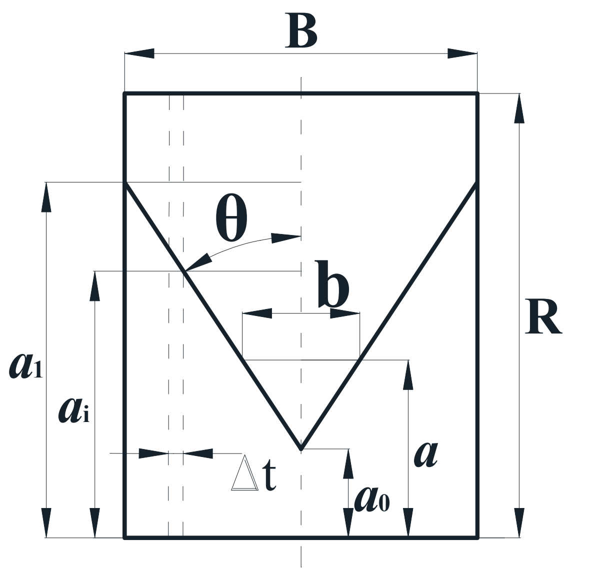

Figure 7. The slice synthetic method for the LCNSCB specimen.

The total load of the LCNSCB specimen is the sum of the central part of the width (b) and the sheet sections on both sides, as shown below:

$$P = \frac{2RbK_{\mathrm{I}}}{Y'(\alpha)\sqrt{\pi a}} + 2\sum_{i=1}^{N} \frac{2R\Delta t K_{\mathrm{I}}}{\beta Y'(\alpha_i)\sqrt{\pi a_i}} \tag{5}$$

The trigonometric function relation of the cutting section of the LCNSCB specimen is:

$$\tan\theta = \frac{B}{2(a_1 - a_0)} = \frac{b}{2(a - a_0)} = \frac{0.5b + i \cdot \Delta t}{(a_i - a_0)} \tag{6}$$

The central crack width (b) can be obtained from the trigonometric function relationship:

$$b = 2\tan\theta(a - a_0) \tag{7}$$

The slice thickness Δt can be determined by the following formula:

$$\Delta t = \frac{B - b}{2N} \tag{8}$$

The dimensionless crack length *ai* can be determined by the trigonometric function relationship:

$$a_i = a_0 + \frac{0.5b + i \cdot \Delta t}{\tan\theta} \tag{9}$$

By introducing the expression P in Formula (5) into Formula (1), the expression of Y^* can be obtained by eliminating K_{I}:

$$Y* = \frac{B}{2}\sqrt{\frac{\pi}{R}}\left[\frac{b}{Y'_{\mathrm{I}}(\alpha)\sqrt{a}} + 2\sum_{i=1}^{N}\frac{\Delta t}{\beta Y'_{\mathrm{I}}(\alpha_i)\sqrt{a_i}}\right]^{-1} \tag{10}$$

$$\beta = 1 + \gamma \frac{\alpha_1 - \alpha}{\alpha_B} \tag{11}$$

The coefficient $\gamma = 0.85$ in Formula (11) is obtained by comparing the simulation results of the finite element in Section 3.1 and the slice synthesis method.

The calculation of Formula (10) is realized by MATLAB programming, and the calculation of $Y^*_{\min}$ is realized by a two-layer loop. The inner loop realizes the accumulation of the N-layer sheet load. The outer loop allows α in 0.01 increments from α_0 to α_1 to facilitate the calculation of Y*. Note that N needs to be large enough to ensure that the three digits after the calculated Y* decimal point remain unchanged. The program calculation can obtain the dimensionless stress intensity factor $Y^*_{\min}$ corresponding to the critical length $\alpha_{\rm m}$.

Reference [31] specifies that the $\alpha = a/R$ value range of Formula (3) is $0.2 \leq a/R \leq 0.8$, and the span diameter ratio is 0.5~0.8. The span ratio of the specimens in this paper is 0.8, which meets the requirements. Due to the special grooving dimensions of this test specimen ($\alpha_0 = 0$ and $\alpha_1 = 1$), a distance around $\alpha_0 = 0$ at the beginning is skipped in the MATLAB program, and calculation is started directly from 0.2, so that α meets the requirements of the range of a/R values in Formula (3). In order to improve the calculation efficiency of the program, skip a distance near the tail $\alpha_1 = 1$. So, set the value range of the α in the program at 0.2~0.8, as shown in Figure 8, which meets the dual requirements of the effective value range of α and efficient program calculation. Figure 9 shows the Y* fitting curve obtained by the slice synthetic method (SSM).

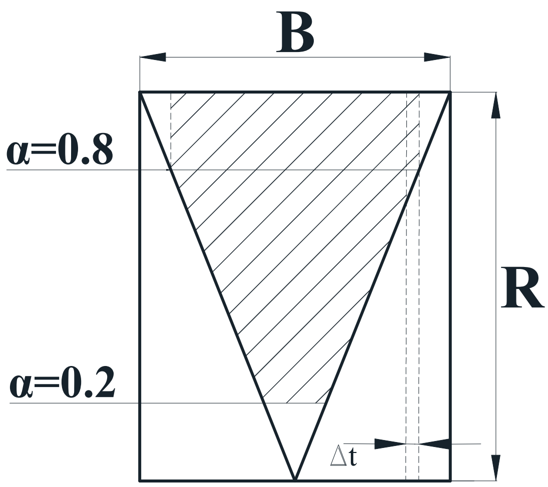

Figure 8. Range of α in MATLAB programming.

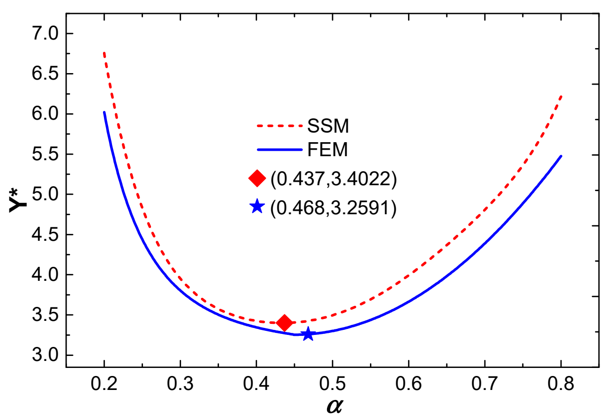

Figure 9. The fitting curve of Y* by SSM and FEM.

3.3. Comparison of the Two Methods

Figure 9 is the two methods obtaining relatively consistent Y^* curves. The trend of change is that with the increase in α, the Y^* decreases first and then increases, which represents the transformation process of steady-state expansion ($\alpha < \alpha_m$) and unsteady expansion ($\alpha > \alpha_m$) of cracks. The finite element method obtained Y^*_{min} = 3.2591 and the slice synthesis method obtained Y^*_{min} = 3.4022, and the latter versus the former, with a deviation of 4.39%.

4. Experimental Analysis and Discussion

4.1. Experimental Result

According to the arrangement of bedding and ligament surface in reference [23], two groups of specimens were designed in this experiment. The vertical intersecting modes of groove ligament and bedding are an arrester arrangement (specimen number h90) and a divider arrangement (specimen number V). Figure 10 shows the morphology of surface fracture and fracture surface fracture after the rupture of two groups of typical specimens. From the surface morphology of the fractured specimens, the cracks of the specimens were extended along the vertical bedding of the precast groove surface, and the specimen is divided into two halves on average. From the fracture morphology of the specimen after rupture, the arrester grooved specimen has a slightly rougher fracture surface and a slightly higher surface undulation than the divider grooved specimen, which has a flatter fracture. Although the fracture surface of the specimen is slightly undulating, the general tendency of the cracks is to expand along the orientation of the maximum principal stress, and the crack path is successfully confined in the vertical plane, which produces a good vertical cracking effect [32]. The fracture does not have left and right deflection and internal torsion, so it is reasonable to believe that the three-point bending experiment was successful and that the measured K_{IC} value was valid.

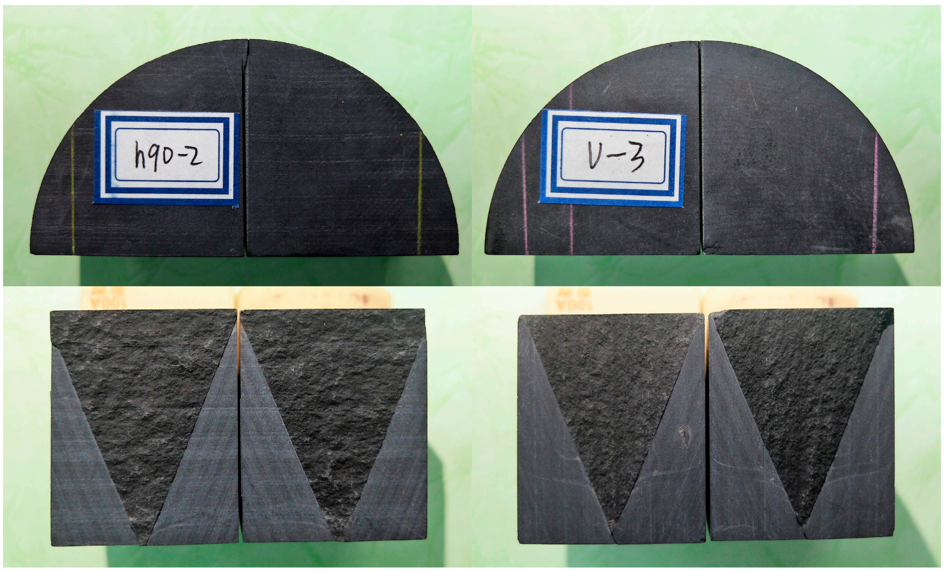

(**a**) **arrester** (**b**) divider

Figure 10. Fracture morphology.

Table 2 shows the peak load P_{max} and fracture toughness K_{IC} calculation results of the LCNSCB specimens under the two notch arrangements. Table 3 is the summary data. Where Y^*_{min} is the result of using the finite element method to calculate, the K_{IC} value is calculated by Formula (1), and the coefficient of variation is the ratio of standard deviation and the mean, which can compare the variation range between each set of data and its own mean. The K_{IC} mean values of h90 (arrester) and V (divider) classes are 1.1998 and 1.2923, and the coefficient of variation are 0.0740 and 0.2362, respectively. The former has a small coefficient of variation and very concentrated data, while the latter has a slightly larger coefficient of variation and more discrete data.

Table 2. K_{IC} values from all tested LCNSCB specimens.

Specimen Number	B/mm	R/mm	Y^*_{min}	P_{max}/kN	K_{IC}/(MPa·m$^{0.5}$)
h90-1	30	37.5	3.2591	2.1676	1.2141
h90-2	30	37.5	3.2591	2.1744	1.2179
h90-3	30	37.5	3.2591	2.3032	1.2901
h90-4	30	37.5	3.2591	1.9234	1.0773
V-1	30	37.5	3.2591	2.4673	1.3820
V-2	30	37.5	3.2591	1.7542	0.9825
V-3	30	37.5	3.2591	2.9945	1.6773
V-4	30	37.5	3.2591	2.0125	1.1272

Table 3. Summary of K_{IC} values of all LCNSCB specimens.

Type	P_{max} Mean/ kN	K_{IC} Mean/ (MPa·m$^{0.5}$)	K_{IC} Standard Deviation/ (MPa·m$^{0.5}$)	K_{IC} Coefficient of Variation
h90	2.1421	1.1998	0.0888	0.0740
V	2.3071	1.2923	0.3052	0.2362

4.2. Analysis and Discussion

The shale sample used in this experiment and the shale sample in reference [33] are from the same collection place and the same batch, so the K_{IC} value calculated in this paper can be compared with the data in reference [33]. The comparison results are credible.

Firstly, the experimental data of the LCNSCB specimen in this paper show that the K_{IC} value of the V type (divider) is slightly larger than the K_{IC} value of the h90 type (arrester), which is consistent with the data of the CCNSCB and CSTSCB specimens in reference [33], as shown in Table 4.

Table 4. Comparison of K_{IC} values of specimens with different types of ligaments.

Grooving Direction	Reference [33] Herringbone Slot CCNSCB	Reference [33] CSTSCB	Straight v-Slot in This Text CCNSCB
Arrester	1.1307	0.7309	1.1998
Divider	1.1894	0.9949	1.2923

Secondly, in the h90 type (arrester) arrangement mode, compared with the herringbone slot CCNSCB specimen in reference [33], the CSTSCB specimen, and the CSTSCB specimen in reference [21], the experimental data of the LCNSCB specimen has a small degree of dispersion and the coefficient of variation is only 0.074, which is much smaller than the coefficient of variation of the comparison object, indicating that the K_{IC} value obtained by this experiment is very accurate. The comparison results are listed in Table 5.

Table 5. Comparison of dispersion of K_{IC} values of specimens with different types of ligaments.

Data Sources	P_{max} Mean/kN	K_{IC} Mean /(MPa·m$^{0.5}$)	K_{IC} Coefficient of Variation
This text LCNSCB	2.1421	1.1998	0.0740
Reference [19] CCNSCB	1.2704	1.1307	0.2530
Reference [19] CSTSCB	1.9310	0.7309	0.1908
Reference [9] CCNBD	9.8220	0.9226	0.0144
Reference [9] CSTSCB	1.4870	0.8297	0.1887

Although the coefficient of variation of the CCNBD data in reference [21] is only 0.0144, the K_{IC} value obtained by this method is 0.9226, which is relatively small compared with the K_{IC} measurement value 1.1998 of the LCNSCB method in this paper. Additionally, for the CSTSCB specimens, both the measured K_{IC} value of 0.8297 in reference [21] and the measured K_{IC} value of 0.7309 in reference [19] are significantly smaller than the measured K_{IC} value in this paper. Only the K_{IC} value of the herringbone slot CCNSCB in reference [33] is 1.1307, which is close to the results in this paper.

The reason for the difference in the calculation results of the different methods mentioned above may be that for the standard specimen recommended by ISRM, the length of the process zone of the CSTSCB and CCNBD specimens is larger, but the length of the process zone of the SR and CB specimens is shorter, which leads to the K_{IC} value obtained by the experiment being smaller than the true fracture toughness value of the material. Scholars have suggested that the effective fracture critical propagation length $a_e = a_c + l_{FPZ}$, including the crack tip process zone, is adopted to estimate the fracture toughness of rock materials accurately [21,33]. According to reference [21], at the moment when the crack expands from the steady state to the unsteady state, the critical crack extension length of the specimen is a_c, which is determined by the finite element method or the slice synthesis method, according to the linear elastic fracture theory. The length l_{FPZ} of the crack tip process zone is related to the type of rock, the shape of the groove ligament of the specimen, and the loading mode of the specimen. The K_{IC} value of rock material is mainly affected by the size of l_{FPZ}. According to the fitting curve of Figure 18 in reference [34], for the CCNBD specimen, the K_a/K_c decreases greatly as the l_{FPZ}/R increases, while the K_a/K_c of the SR and CB specimens does not change significantly, and there is no such rule. K_a is the apparent fracture toughness value obtained by experiments and K_c represents the fracture toughness value of the inherent properties of the material, which is obtained from the critical effective crack length a_e. It is shown that with the increase in the fracture process zone, for the CCNBD specimen, the difference between the apparent fracture toughness value and the true fracture toughness value obtained by the experimental test becomes larger, but for the SR and CB specimens, the difference is not obvious. The experimental data of some scholars also confirmed the above rule. In the experimental data of Cui Zhendong [16], for sandstone specimens with diameters of 50, 55, 68, and 74 mm, the K_{IC} values obtained with the SR specimens are 2.59, 2.41, 2.57, and 3.07 $\text{Mpa} \cdot \text{m}^{0.5}$, and the K_{IC} values obtained with the CCNBD specimens are 0.39, 0.63, 1.66, and 1.89 $\text{Mpa} \cdot \text{m}^{0.5}$, respectively. Erarslan's experimental results show that the SR and CCNBD specimens for risbanetuff-1 rock have K_{IC} values of 2.13 and 1.12 $\text{Mpa} \cdot \text{m}^{0.5}$, respectively [35].

Thirdly, the coefficient of variation of the LCNSCB specimen in this experiment of type V (divider) is larger than that of type h90 (arrester), and the reason why the K_{IC} measured value is relatively discrete can be explained with reference to the schematic diagram 10. The crack expansion in the layered specimen is show in Figure 11. According to the calculation principle of the slice synthesis method in Section 3.2 of this paper, it can be known that when the crack extends to the critical length $a_c = a_m$, the part with the middle width (b) plays a major role in calculating the fracture toughness of the specimen. At a certain scale, the shale grain layer composed of different attribute particles is interphase distribution [36,37]. The number of layers included in the central section of the width (b) along the normal direction of the bedding in the arrester mode is greater than the divider. The strength of type V (divider) specimens is only affected by a small amount of bedding. Because the bedding strength of different categories is relatively large, its strength is significantly affected by the bedding strength, showing a large dispersion. However, the strength of h90 (arrester) specimens is affected by the average strength of each bedding because of the large number of grain layers, and the numerical fluctuation degree is smaller than that of the former.

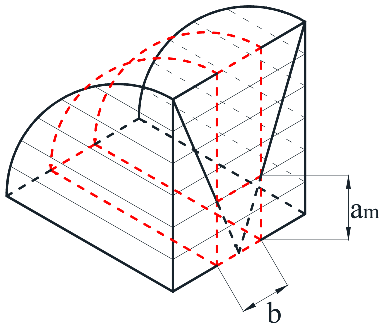

(**a**) arrester

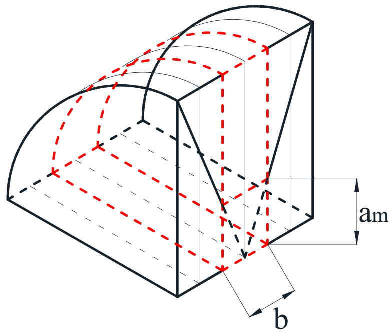

(**b**) divider

Figure 11. Crack expansion in the layered specimen.

5. Conclusions

In the paper, a semi-circular bending specimen with a linear chevron notch ligament (LCNSCB) was designed to accurately test the K_{IC} of the vertical stratification direction of the shale. Two sets of prefabricated samples of LCNSCB specimens under arrester and divider modes were adopted in the three-point bending loading experiments. The following conclusions were obtained:

(1) The minimum dimensionless stress intensity factor ($Y^*{}_{min}$) of the LCNSCB specimen was calculated by the finite element method and the slice synthesis method, respectively. With the increase in α, the Y^* decreases first and then increases, which represents the transformation process of steady-state expansion ($\alpha < \alpha_m$) and unsteady expansion ($\alpha > \alpha_m$).

(2) Compared with the experimental data of the existing literature, these data in this experiment show that the LCNSCB specimen can avoid the disadvantage of lower measured K_{IC} values due to a larger fracture processing zone featured in CSTSCB and CCNBD specimens, combined with the merits of a shorter fracture processing zone of the SR or CR specimens, and the render measured the K_{IC} value to be closer to the material's true fracture toughness value.

(3) The narrow ligament of the LCNSCB specimen has a favorable crack propagation guiding effect and can generate consistent K_{IC} values and could be used to accurately test the fracture toughness of rock material in vertical bedding direction.

(4) The K_{IC} mean values of h90 (arrester) and V (divider) are 1.1998 and 1.2923, and the variation coefficients are 0.0740 and 0.2362, respectively. The latter has a slightly larger variation coefficient and more discrete data.

Author Contributions: Conceptualization, H.W.; methodology, Z.Z.; software, Z.C.; validation, W.Z.; formal analysis, J.L.; investigation, H.Z.; writing-original draft preparation, Z.Z. and H.W.; writing-review and editing, H.W.; funding acquisition, H.W. and Z.C. All authors have read and agreed to the published version of the manuscript.

Funding: This work was financially supported by the National Natural Science Foundation of China (grant number 41972296 and 41807254), the China Postdoctoral Science Foundation (grant number 2020M682372), the Young Talent Support Project of Henan Province (grant number 2021HYTP013), the Key Research & Development and promotion projects of Henan Province (grant number 212102310374), and the technology innovation project of the China Railway Bridge Engineering Bureau Group Co., Ltd. (grant number DQJ-2022-B03).

Institutional Review Board Statement: Not applicable.

Informed Consent Statement: Not applicable.

Data Availability Statement: The data used to support the findings of this study are included in the article.

Conflicts of Interest: The authors declare no conflict of interest.

References

1. Atkinson, B. *Fracture Mechanics of Rock*; Academic Press: London, UK, 1987.
2. Hillerborg, A.; Modeer, M.; Petersson, P.E. Analysis of crack formation and crack growth in concrete by mean of fracture mechanics and finite elements. *Cem. Concr. Res.* **1976**, *6*, 773–782. [CrossRef]
3. Hoover, C.G.; Bažant, Z.P. Universal size-shape effect law based on comprehensive concrete fracture tests. *J. Eng. Mech.-ASCE* **2014**, *140*, 473–479. [CrossRef]
4. Issa, M.A.; Issa, M.A.; Islam, M.S.; Chudnovsky, A. Size effects in concrete fracture: Part I, experimental setup and observations. *Int. J. Fract.* **2000**, *102*, 1–24. [CrossRef]
5. Fang, H.Y. Cracking and fracture behavior of soil. Fracture Mechanics Applied to Geotechnicl Engineering. In Proceedings of the ASCE, Atlanta, GA, USA, 9–13 October 1994; pp. 102–117.
6. Buller, D.; Hughes, S.; Market, J.; Petre, E.; Spain, D.; Odumosu, T. Petrophysical evaluation for enhancing hydraulic stimulation in horizontal shale gas wells. In Proceedings of the SPE Annual Technical Conference and Exhibition, Florence, Italy, 19–22 September 2010; p. 132990.
7. Hucka, V.; Das, B. Brittleness determination of rocks by different methods. *Int. J. Rock Mech. Min. Sci. Geomech. Abstr. Pergamon* **1974**, *11*, 389–392. [CrossRef]
8. Xu, S.; Malik, M.A.; Li, Q.; Wu, Y. Determination of double-K fracture parameters using semi-circular bend test specimens. *Eng. Fract. Mech.* **2016**, *152*, 58–71. [CrossRef]
9. Oh, S.W.; Min, G.J.; Park, S.W.; Kim, M.S.; Obara, Y.; Cho, S.H. Anisotropic influence of fracture toughness on loading rate dependency for granitic rocks. *Eng. Fract. Mech.* **2019**, *221*, 106677. [CrossRef]
10. Kataoka, M.; Obara, Y.; Kuruppu, M. Estimation of fracture toughness of anisotropic rocks by semi-circular bend (SCB) tests under water vapor pressure. *Rock Mech. Rock Eng.* **2015**, *48*, 1353–1367. [CrossRef]
11. Nasseri MH, B.; Grasselli, G.; Mohanty, B. Fracture toughness and fracture roughness in anisotropic granitic rocks. *Rock Mech. Rock Eng.* **2010**, *43*, 403–415. [CrossRef]
12. Wang, Y.; Tan, P.F.; Han, J.; Li, P. Energy-driven fracture and instability of deeply buried rock under triaxial alternative fatigue loads and multistage unloading conditions: Prior fatigue damage effect. *Int. J. Fatigue* **2023**, *168*, 107410. [CrossRef]
13. Wang, Y.; Su, Y.; Xia, Y.; Wang, H.; Yi, X. On the effect of confining pressure on fatigue failure of block-in-matrix soils exposed to multistage cyclic triaxial loads. *Fatigue Fract. Eng. Mater. Struct.* **2022**, *45*, 2481–2498. [CrossRef]
14. Wang, Y.; Mao, T.; Xia, Y.; Li, X.; Yi, X. Macro-meso fatigue failure of bimrocks with various block content subjected to multistage fatigue triaxial loads. *Int. J. Fatigue* **2022**, *163*, 107014. [CrossRef]
15. Nejati, M.; Bahrami, B.; Ayatollahi, M.R.; Driesner, T. On the anisotropy of shear fracture toughness in rocks. *Theor. Appl. Fract. Mech.* **2021**, *113*, 102946. [CrossRef]
16. Cui, Z.-D.; Liu, D.-A.; An, G.-M.; Sun, B.; Zhou, M.; Cao, F.-Q. A comparison of two ISRM suggest-ed chevron notched specimens for testing mode-I rock fracture toughness. *Int. J. Rock Mech. Min. Sci.* **2010**, *47*, 871–876. [CrossRef]
17. Franklin, J.A.; Sun, Z.Q.; Atkinson, B.K.; Meredith, P.G.; Bobrov, G.F. Suggested methods for determining the fracture toughness of rock. *Int. J. Rock Mech. Min. Sci. Geomech. Abstr.* **1988**, *25*, 71–96.
18. Backers, T.; Stephansson, O. ISRM suggested method for the determination of mode II fracture toughness. *Rock Mech Rock Eng.* **2012**, *45*, 1011–1022. [CrossRef]
19. ISRM. The complete ISRM suggested methods for rock characterization, testing and monitoring: 1974–2006. In *Suggested Methods Prepared by the Commission on Testing Methods*; compilation arranged by the ISRM Turkish National Group; Ulusay, R., Hudson, J.A., Eds.; International Society for Rock Mechanics: Ankara, Turkey, 2007.
20. Kuruppu, M.D.; Obara, Y.; Ayatollahi, M.R.; Chong, K.P.; Funatsu, T. ISRM-Suggested Method for Determining the Mode I Static Fracture Toughness Using Semi-Circular Bend Specimen. *Rock Mech. Rock Eng.* **2014**, *47*, 267–274. [CrossRef]
21. Wang, H.; Zhao, F.; Huang, Z.; Yao, Y.; Yuan, G. Experimental study of mode-I fracture toughness for layered shale based on two ISRM-suggested methods. *Rock Mech. Rock Eng.* **2017**, *50*, 1933–1939.
22. Wang, H.; Liu, D.; Cui, Z.; Cheng, C.; Jian, Z. Investigation of the fracture modes of red sandstone using XFEM and acoustic emissions. *Theor. Appl. Fract. Mech.* **2016**, *85*, 283–293. [CrossRef]
23. Zhao, Z.; Wang, H.; Cui, Z.; Zhao, F.; Tang, T.; Han, W.; Wang, X. Experimental study on Mode-I fracture toughness using Chevron Straight-notched Semi-circular Bend (CSNSCB) method. *Theor. Appl. Fract. Mech.* **2021**, *116*, 103093. [CrossRef]
24. Wang, H.; Zhao, F.; Huang, Z.; Yu, H.; Niu, J.; Zhang, P. Study on acoustic emission characteristics of sandstone under different fracture modes. *Arab. J. Geosci.* **2018**, *11*, 772. [CrossRef]
25. Fowell, R.J.; Hudson, J.A. Suggested method for determining mode I fracture toughness using cracked chevron notched Brazilian disc (CCNBD) specimens. *Int. J. Rock Mech. Min. Sci. Geomech. Abstr.* **1995**, *32*, 57–64. [CrossRef]
26. Chen, J.F. The development of the cracked-chevron-notched Brazilian disc methods for rock fracture toughness measurement. In Proceedings of the SEM Spring Conference on Experimental Mechanicsm, Albuquerque, NM, USA, 4–6 June 1990.
27. Wang, Q.Z.; Jia, X.M.; Kou, S.Q.; Zhang, Z.X.; Lindqvist, P.A. More accurate stress intensity factor derived by finite element analysis for the ISRM suggested rock fracture toughness specimen CCNBD. *Int. J. Rock Mech. Min. Sci.* **2003**, *40*, 233–241. [CrossRef]
28. Bluhm, J.I. Slice synthesis of a three dimensional work of fracture specimen. *Eng. Fract. Mech.* **1975**, *7*, 593–604. [CrossRef]

29. Xu, C.; Fowell, R.J. Stress intensity factor evaluation for cracked chevron notched brazilian disc specimens. *Int. J. Rock Mech. Min. Sci. Geomech. Abstr.* **1994**, *31*, 157–162. [CrossRef]
30. Wang, Q.Z.; Jia, X.M.; Wu, L.Z. Wide-range stress intensity factors for the ISRM suggested method using CCNBD specimens for rock fracture toughness tests. *Int. J. Rock Mech. Min. Sci.* **2004**, *41*, 709–716. [CrossRef]
31. Ayatollahi, M.R.; Mahdavi, E.; Alborzi, M.J.; Obara, Y. Stress Intensity Factors of Semi-Circular Bend Specimens with Straight-through and Chevron Notches. *Rock Mech. Rock Eng.* **2016**, *49*, 1161–1172. [CrossRef]
32. Tutluoglu, L.; Keles, C. Mode I fracture toughness determination with straight notched disk bending method. *Int. J. Rock Mech. Min. Sci.* **2011**, *48*, 1248–1261. [CrossRef]
33. Zhao, Z.-J.; Liu, D.-A.; Cui, Z.-D.; Tang, T.-W. Experimental study of determining fracture toughness KIC of shale by semi-disk three-point bending. *Rock Soil Mech.* **2018**, *39*, 267–275.
34. Wei, M.D.; Dai, F.; Xu, N.W.; Zhao, T. Stress intensity factors and fracture process zones of ISRM-suggested chevron notched specimens for mode I fracture toughness testing of rocks. *Eng. Fract. Mech.* **2016**, *168*, 174–189. [CrossRef]
35. Erarslan, N. A Study on the Evaluation of the Fracture Process Zone in CCNBD Rock Samples. *Exp. Mech.* **2013**, *53*, 1475–1489. [CrossRef]
36. Lee, H.P.; Olson, J.E.; Holder, J.; Gale, J.F.; Myers, R.D. The interaction of propagating opening mode fractures with preexisting discontinuities in shale. *J. Geophys. Res. Solid Earth* **2015**, *120*, 169–181. [CrossRef]
37. Li, L.H.; Huang, B.X.; Tan, Y.F. Geometric Heterogeneity of Continental Shale in the Yan-chang Formation, Southern Ordos Basin, China. *Sci. Rep.* **2017**, *7*, 6006. [CrossRef]